Data driving the top quark forward-backward asymmetry with a lepton-based handle

Adam Falkowski,[1,*] Michelangelo L. Mangano,[2,†] Adam Martin,[2,3,‡,¶] Gilad Perez,[2,4,§] and Jan Winter[5,2,‖]

[1]*Laboratoire de Physique Theorique d'Orsay, UMR8627-CNRS, Universite Paris-Sud, Orsay, France*
[2]*PH-TH Department, CERN, CH-1211 Geneva 23, Switzerland*
[3]*Department of Physics, University of Notre Dame, Notre Dame, Indiana 46556, USA*
[4]*Department of Particle Physics and Astrophysics, Weizmann Institute of Science, Rehovot 76100, Israel*
[5]*Max-Planck-Institute for Physics, Föhringer Ring 6, D-80805 Munich, Germany*

(Received 9 January 2013; published 27 February 2013)

We propose that, within the standard model, the correlation between the $t\bar{t}$ forward-backward asymmetry $A_{t\bar{t}}$ and the corresponding lepton-based asymmetry A_l—at the differential level—is strong and rather clean both theoretically and experimentally. Hence a combined measurement of the two distributions as a function of the lepton p_T, a direct and experimentally clean observable, would lead to a potentially unbiased and normalization-free test of the standard model prediction. To check the robustness of our proposal, we study how the correlation is affected by mismeasurement of the $t\bar{t}$ system transverse momenta, acceptance cuts, and scale dependence and compare the results of MCFM, POWHEG (with and without PYTHIA showering), and SHERPA's CSSHOWER in first-emission mode. We find that the shape of the relative differential distribution $A_l(p_T^l)[A_{t\bar{t}}(p_T^l)]$ is only moderately distorted, hence supporting the usefulness of our proposal. Beyond the first emission, we find that the correlation is not accurately captured by lowest-order treatment. We also briefly consider other differential variables such as the system transverse mass and the canonical $t\bar{t}$ invariant mass. Finally, we study new physics scenarios where the correlation is significantly distorted and therefore can be more readily constrained or discovered using our method.

DOI: 10.1103/PhysRevD.87.034039 PACS numbers: 14.65.Ha, 13.85.Rm

I. INTRODUCTION

Within the standard model (SM), the $t\bar{t}$ forward-backward asymmetry, $A_{t\bar{t}}$, is an interesting variable because it tells us about QCD interactions beyond leading order but in a region that should be well described by perturbation theory [1,2]. Furthermore, as the standard model contributions are expected to be small [1–5], the measurement of $A_{t\bar{t}}$ is sensitive to beyond-the-SM (BSM) contributions. The asymmetry is quite a unique observable since shifting it requires new physics with nonstandard couplings both to the $t\bar{t}$ quark current as well as to the to the current of $u\bar{u}$ (or possibly $d\bar{d}$) initial-state quarks.[1]

The current status of top quark asymmetry related measurements at the Tevatron is intriguing. It is useful to classify the current data into measurements that directly probe the $t\bar{t}$ asymmetries and measurements that probe daughter asymmetries, such as the lepton-based ones. The asymmetries are quoted at several different stages of the analysis. The easiest number to compare with theory is the ''unfolded,'' or ''production level,'' asymmetry, where the collaborations have processed the measured asymmetry to remove background contamination and the effects of analysis cuts and the detector. Both CDF [6,7] (9.4 fb^{-1}) and DØ [8] (5.4 fb^{-1}) present their inclusive semileptonic $t\bar{t}$ asymmetry results at this level. The average of the two measurements is

$$A_{t\bar{t}} = 0.174 \pm 0.038, \tag{1}$$

which is significantly larger than the SM prediction,

$$A_{t\bar{t}}^{\mathrm{SM}} = 0.088 \pm 0.006, \tag{2}$$

obtained from next-to-leading order (NLO) QCD and including the leading electroweak (EW) contributions [1,2,9–11]. The SM prediction is derived taking the leading-order total cross section in the denominator of the asymmetry—a conservative approach—and the error on the SM prediction has been estimated by varying renormalization and factorization scales (see e.g., Ref. [12]).

Both CDF and DØ have also measured the dependence of the asymmetry on the mass and rapidity of the $t\bar{t}$ system. For the $m_{t\bar{t}}$ dependence, CDF [6,7,13] finds, after unfolding,

$$\begin{aligned} A_{t\bar{t}}^{\mathrm{low}} &\equiv A_{t\bar{t}}(m_{t\bar{t}} < 450\ \mathrm{GeV}) = 0.084 \pm 0.053, \\ A_{t\bar{t}}^{\mathrm{high}} &\equiv A_{t\bar{t}}(m_{t\bar{t}} > 450\ \mathrm{GeV}) = 0.295 \pm 0.066. \end{aligned} \tag{3}$$

The asymmetry in the high-$m_{t\bar{t}}$ bin is particularly striking given that the SM prediction, including EW corrections [1,2,9–11], is much lower,

*adam.falkowski@th.u-psud.fr
†michelangelo.mangano@cern.ch
‡adam.martin@cern.ch
§gilad.perez@cern.ch
‖jan.winter@cern.ch
¶Visiting scholar.

[1]Flavor-violating, t-channel new physics mechanisms to shift $A_{t\bar{t}}$ can be Fierz rearranged into a form where this is true.

$$\left(A_{t\bar{t}}^{\text{high}}\right)^{\text{SM}} \equiv 0.129^{+0.008}_{-0.006}. \tag{4}$$

For the same quantity, DØ has only reported a measurement without unfolding (''reconstruction level''),

$$\left(A_{t\bar{t}}^{\text{high}}\right)_{\text{reco}} = 0.115 \pm 0.060. \tag{5}$$

We note that the DØ value for $A_{t\bar{t}}^{\text{high}}$ is consistent with the CDF value at the reconstruction level, $(A_{t\bar{t}}^{\text{high}})_{\text{reco}} = 0.198 \pm 0.043$, which suggests that upon unfolding, the value obtained by DØ would be larger than the SM expectation. Putting it differently, assuming the same unfolding factor between CDF and DØ, we find that both measurements prefer a rather large value for $A_{t\bar{t}}^{\text{high}}$, but with DØ being more consistent with the SM prediction.

The other class of forward-backward asymmetric observables is the lepton-based asymmetries. From the same selected events used to measure $A_{t\bar{t}}$, both Tevatron experiments have also measured the single, A_l, and dilepton, A_{ll}, asymmetries [8,13–15]. The results, given at the unfolded level,[2] are

$$\begin{aligned}(A_l)_{\text{CDF}} &= 0.066 \pm 0.025,\\ (A_{ll})_{\text{CDF}} &= 0.42 \pm 0.15 \pm 0.050,\end{aligned} \tag{6}$$

$$\begin{aligned}(A_l)_{\text{D}\emptyset} &= 0.152 \pm 0.04,\\ (A_{ll})_{\text{D}\emptyset} &= 0.053 \pm 0.084.\end{aligned} \tag{7}$$

The SM predictions for the leptonic asymmetries, as reported by the experimental collaborations, are

$$\begin{aligned}(A_l)^{\text{SM}}_{\text{CDF}} &= 0.016,\\ (A_{ll})^{\text{SM}}_{\text{CDF}} &= 0.060 \pm 0.01,\end{aligned} \tag{8}$$

$$\begin{aligned}(A_l)^{\text{SM}}_{\text{D}\emptyset} &= 0.021 \pm 0.001,\\ (A_{ll})^{\text{SM}}_{\text{D}\emptyset} &= 0.047 \pm 0.001.\end{aligned} \tag{9}$$

Being a proton-proton collider, the LHC is not sensitive to $A_{t\bar{t}}$. However, the LHC can probe a related observable—the charge asymmetry in $t\bar{t}$ production, A_C. Measurements of A_C at $\sqrt{s} = 7$ TeV have been reported by both ATLAS [16] (for 4.7 fb^{-1}) and CMS [17,18] (for 5.0 fb^{-1}). The expected SM asymmetry [1,2,11], $A_C^{\text{SM}} = 0.0115 \pm 0.0006$, is much smaller than the Tevatron's asymmetries, due to the domination of the gluon-gluon production channel, which is symmetric. The LHC measurements so far are consistent with the SM value, but the size of the statistical and systematic uncertainties is such that one cannot yet exclude the consistency with the anomalous Tevatron $A_{t\bar{t}}$ result. It is important to emphasize that even within the SM, the Tevatron and LHC observables differ in nature. In particular, the dominant $t\bar{t}$ production mechanism and the kinematical reaches available to the top quarks are clearly very different at the two colliders; the Tevatron collides charge-asymmetric beams, and top quark production is dominated by quark-antiquark annihilation, while at the LHC, collisions are charge symmetric, and top pair production is driven by gluon-gluon collisions. Furthermore, non-SM dynamics can naturally induce a large deviation for the forward-backward asymmetry at the Tevatron without affecting the charge asymmetry at the LHC [12,19–21].

Given that the LHC probes a different observable, we turn our attention back to the Tevatron. The discrepancy between the SM predictions and the measured asymmetries at the Tevatron could be due to an unknown QCD effect, or an unidentified experimental bias. Alternatively, it might be a hint of dynamics beyond the SM (for a review, see e.g., Ref. [22]). Either way, the current situation is not satisfying, and the main goal of this paper is to investigate what other information can be used to gain more insight. Specifically, we propose a correlation between $A_{t\bar{t}}$ and daughter asymmetries that are experimentally easy to measure and also under theoretical control. This correlation can then be used to distinguish the SM from more exotic explanations of $A_{t\bar{t}}$.

Our basic idea is simple, at least in principle. In the SM, the lepton-based asymmetry in $t\bar{t}$ events is completely determined by the $t\bar{t}$ asymmetry, meaning for a given $A_{t\bar{t}}$ one can use top quark decay kinematics to predict A_l. Radiation originating from the top quark decay products alters the kinematics and blurs the relationship between A_l and $A_{t\bar{t}}$, however this effect is suppressed by the narrow width of the top quark. This relationship is true for the inclusive asymmetries, but also differentially—taking the asymmetries with respect to a kinematic variable x; in each bin of x, the lepton asymmetry can be fixed knowing $A_{t\bar{t}}$ in that bin, such that $A_l(x)[A_{t\bar{t}}(x)]$ traces a calculable curve as x is varied.

However, once we move beyond the SM, A_l and $A_{t\bar{t}}$ are generically independent. At high $m_{t\bar{t}}$, A_l is indeed driven by the top quark kinematics and polarization [23–29], however, near the $t\bar{t}$ threshold, A_l is set by the initial-state quark polarization rather than anything related to the top quarks [30]. Thus, given some observable x that interpolates between the threshold and high-$m_{t\bar{t}}$ regions (lepton p_T, H_T, etc.), the curve $A_l(x)$ versus $A_{t\bar{t}}(x)$ will be different for models beyond the SM. Our proposal is to use $x = p_T^l$ (the lepton p_T) and to simultaneously measure $A_l(p_T^l)$ and $A_{t\bar{t}}(p_T^l)$, to verify whether the curve $A_l(p_T^l)$ $[A_{t\bar{t}}(p_T^l)]$ is in agreement with the SM. We choose the lepton p_T as our kinematic variable because it is experimentally clean and easy to reconstruct.

We begin our study of this correlation in Sec. II, working at the parton level and without cuts to demonstrate the basic idea. In Sec. II A. we provide several checks that suggest that the correlation is indeed robust and therefore more sensitive to new physics contributions to the asymmetries.

[2]Note that the CDF Collaboration has not yet published an unfolded result for A_l, the one we state here is given for events at the ''background-subtracted level.''

In detail, we consider the following three types of effects: (1) mismodeling of the of the $t\bar{t}$ transverse momenta, (2) scale dependence of the differential asymmetries, and (3) radiation in the top decay. We verify that while some of these effects influence the overall normalization of the asymmetries, affecting the agreement between theory and experiment, the correlation between $A_l(p_T^l)$ and $A_{t\bar{t}}(p_T^l)$ is unaffected by these deformations. Then, in Sec. III we include detector acceptance, experimental cuts, parton showering, and top quark reconstruction to show the asymmetry correlation in a realistic hadron-collider environment. Finally, in Sec. IV we consider several simple new physics models and show that the SM correlation is significantly violated in general which therefore can potentially lead to much cleaner extraction of a possible non-SM signal. This is followed by some discussion regarding the use of reconstruction-free variables (Sec. V) and our conclusions (Sec. VI).

II. IDEALIZED CASE: SM

To get some insight regarding our proposal, we begin by discussing the idealized SM case where no acceptance cuts are included. The differential asymmetry observables are defined as

$$A_{t\bar{t}}(p_T^l) = \frac{N_{\Delta Y_{t\bar{t}}>0}(p_T^l) - N_{\Delta Y_{t\bar{t}}<0}(p_T^l)}{N_{\Delta Y_{t\bar{t}}>0}(p_T^l) + N_{\Delta Y_{t\bar{t}}<0}(p_T^l)}, \tag{10}$$

$$A_l(p_T^l) = \frac{N_{Y_l>0}(p_T^l) - N_{Y_l<0}(p_T^l)}{N_{Y_l>0}(p_T^l) + N_{Y_l<0}(p_T^l)}, \tag{11}$$

where $N_{\Delta Y_{t\bar{t}}>0}$ ($N_{Y_l>0}$) and $N_{\Delta Y_{t\bar{t}}<0}$ ($N_{Y_l<0}$) are the number of events with $\Delta Y_{t\bar{t}}$ (Y_l) greater or less than zero.[3] We also study the cumulative distributions—the asymmetry for all events with lepton p_T above a given threshold, obtainable by integrating the numerator and denominator of the differential distributions, then taking the ratio

$$A_{t\bar{t}}(p_{T,\mathrm{cut}}^l) = \frac{\int_{p_{T,\mathrm{cut}}}^{\infty}(N_{\Delta Y_{t\bar{t}}>0}(p_T^l) - N_{\Delta Y_{t\bar{t}}<0}(p_T^l))}{\int_{p_{T,\mathrm{cut}}}^{\infty}(N_{\Delta Y_{t\bar{t}}>0}(p_T^l) + N_{\Delta Y_{t\bar{t}}<0}(p_T^l))}, \tag{12}$$

$$A_l(p_{T,\mathrm{cut}}^l) = \frac{\int_{p_{T,\mathrm{cut}}}^{\infty}(N_{Y_l>0}(p_T^l) - N_{Y_l<0}(p_T^l))}{\int_{p_{T,\mathrm{cut}}}^{\infty}(N_{Y_l>0}(p_T^l) + N_{Y_l<0}(p_T^l))}. \tag{13}$$

The differential distributions contain the physics we want to study—the correlation between A_l and $A_{t\bar{t}}$, but they are difficult to measure experimentally owing to the limited top quark sample size. Meanwhile, cumulative distributions are more tractable experimentally, but the integration over multiple bins dilutes the correlation between $A_{t\bar{t}}$ and A_l. We present both types of distributions for the idealized SM case to show the similarities and differences.

We are interested in the lepton asymmetry in the lab frame, as well as the lepton asymmetry after boosting to a frame where the $t\bar{t}$ system has no longitudinal momentum. The lepton kinematics, which encode the asymmetry inherited from the top quarks, get smeared under motion of the $t\bar{t}$ system, hence boosting back leads to a larger A_l. The boost only effects the leptonic asymmetry, as $A_{t\bar{t}}$ is defined in terms of a rapidity difference and is manifestly invariant under longitudinal boosts. Unless otherwise specified, we will use the generic A_l for the lab frame lepton asymmetry A_l^{lab}, and use A_l^{boost} to refer specifically to the lepton asymmetry in the boosted frame.

The primary tools for our study are the NLO Monte Carlo generators MCFM (v6.3) [31,32], and POWHEG (here run in the hardest-emission generator mode) using the heavy quark production routines [33–36]. For the idealized SM case, all results were generated using the MSTW2008NLO [37] parton distribution functions and with factorization and renormalization scales set to $\mu_{\mathrm{R}} = \mu_{\mathrm{F}} = Q = \sqrt{m_t^2 + (p_T^t)^2}$. Spin correlations between the top (antitop) quark and its corresponding decay products are maintained in both codes.[4]

The distributions $A_{t\bar{t}}(p_T^l)$, $A_l(p_T^l)$, $A_{t\bar{t}}(p_{T,\mathrm{cut}}^l)$, and $A_l(p_{T,\mathrm{cut}}^l)$ for the ideal case are shown below in Fig. 1. The darker lines show the MCFM results, while the results obtained with POWHEG are shown in the lighter shaded lines. The green curves show $A_l(p_T^l)$ in the lab frame, while the red curves show $A_l^{\mathrm{boost}}(p_T^l)$, the lepton asymmetry in the $Y_{t\bar{t}} = 0$ frame. We find that the two NLO Monte Carlo (MC) generators are in reasonable agreement. The qualitative behavior of the curves can be understood as follows: beginning with the leptonic asymmetries, near threshold $A_l(p_T^l)$ is sensitive to the polarization of the incoming quark, which is small due to the vectorlike nature of QCD. Hence we expect A_l to be near zero [30]. In the other extreme limit, when the lepton's p_T is very large it has to come from a boosted top quark, and therefore the lepton-based asymmetry should asymptote to the corresponding value of $A_{t\bar{t}}$, keeping in mind that within the SM no net polarization is expected for the top quarks in $t\bar{t}$ events. This is consistent with the lepton-based asymmetry curves shown in the plot.

The behavior of $A_{t\bar{t}}(p_T^l)$ can be understood from the lepton p_T spectrum in $t\bar{t}$ events and the dependence of $A_{t\bar{t}}$ on $m_{t\bar{t}}$. The asymmetry $A_{t\bar{t}}(m_{t\bar{t}})$ is a monotonically increasing function of $m_{t\bar{t}}$ (see Fig. 2 where for completeness $A_{t\bar{t}}(m_{t\bar{t}})$ and $A_l(m_{t\bar{t}})$ are presented) [5,38,39], however $m_{t\bar{t}}$ is only weakly correlated with p_T^l (at least up to $p_T^l \lesssim 100$ GeV). The correlation, at leading order (LO), between these variables is shown explicitly in Fig. 3. The

[3] Y_l is defined as $Q_l \cdot \eta_l$, such that a backwards-moving electron is the same as a forwards-moving positron.

[4] Other relevant choices of Monte Carlo generation parameters are $m_t = 173$ GeV, $\Gamma_t = 1.31$ GeV, and $m_b = 5.0$ GeV.

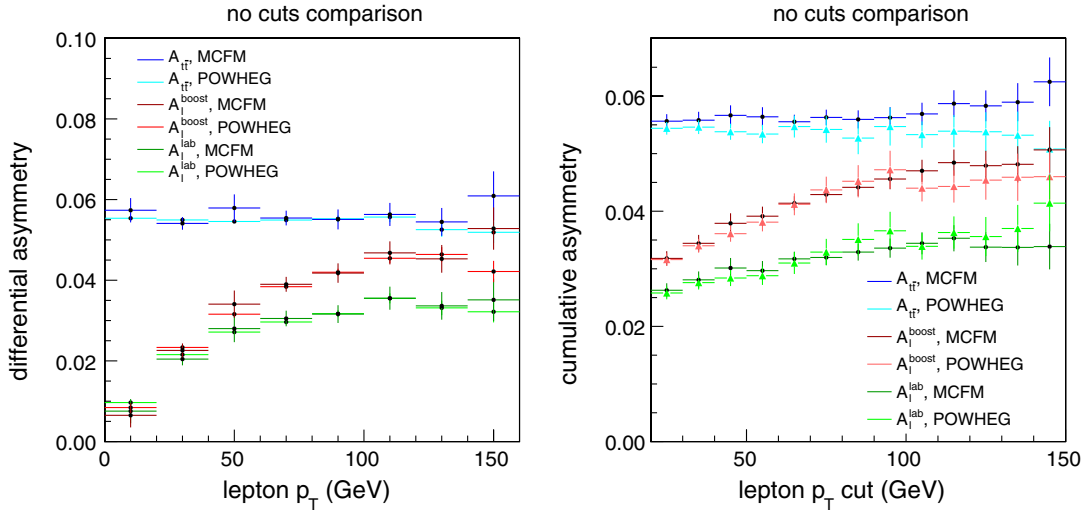

FIG. 1 (color online). The dependence of top quark and leptonic asymmetries on the lepton p_T. The left panel shows the differential distributions $A_{t\bar{t}}(p_T^l)$, $A_l(p_T^l)$ for the SM ideal case, while the cumulative asymmetries $A_{t\bar{t}}(p_{T,\mathrm{cut}}^l)$, $A_l(p_{T,\mathrm{cut}}^l)$ are shown in the right hand panel. The darker lines depict the MCFM results, while the results obtained with POWHEG are shown in the lighter shaded lines. The green curves show A_l in the lab frame, while the red curves show A_l after boosting to a frame where the $t\bar{t}$ system has no longitudinal momentum. This boost only affects the leptonic asymmetries.

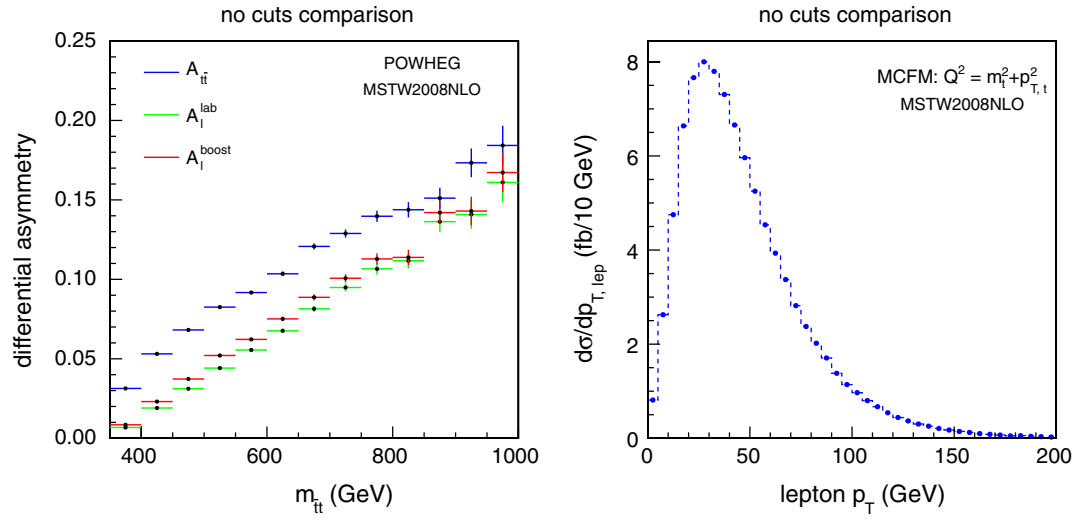

FIG. 2 (color online). The differential asymmetries $A_{t\bar{t}}(m_{t\bar{t}})$, $A_l(m_{t\bar{t}})$ for the SM ideal case are shown in the left panel. The lepton p_T distribution (at LO) is shown in the right panel, normalized to the total cross section.

weakness of the $m_{t\bar{t}} - p_T^l$ correlation implies that the lower p_T^l bins are populated almost equally by a wide range of invariant masses and hence we do not expect a significant rise in $A_{t\bar{t}}(p_T^l)$ as the lepton p_T is varied.[5]

Higher p_T^l events are more correlated with large $m_{t\bar{t}}$, however the large lepton transverse momenta, which naively would lead to a large $A_{t\bar{t}}$, are forcing those energetic events to be central. As shown in Fig. 3, events with $p_T^l \gtrsim 150$ GeV have $m_{t\bar{t}} \gtrsim 550$ GeV, however, with a top quark rapidity difference below 0.7 (as shown in Fig. 3 visualizing the correlation between $\Delta Y_{t\bar{t}}$ and p_T^l). As central events tend to have lower $A_{t\bar{t}}$, we actually expect the overall value of $A_{t\bar{t}}$ and A_l to be below their nominal value expected based on the inclusive and high invariant mass values prior to lepton transverse momenta cuts (Fig. 2). This is consistent with the distributions shown in Fig. 1.

We close this subsection by presenting the same result but this time on the $A_l - A_{t\bar{t}}$ plane, where each point in the

[5]A similar argument for the flatness of $A_{t\bar{t}}(p_T^l)$ can be made using the $Y_{t\bar{t}} - p_T^l$ correlation (at LO) depicted in the right panel of Fig. 3. The differential asymmetry $A_{t\bar{t}}(|Y_{t\bar{t}}|)$ rises monotonically/linearly for increasing absolute values of $Y_{t\bar{t}}$, and from Fig. 3 we see that each p_T^l bin picks events with a variety of $Y_{t\bar{t}}$ values. The asymmetry in a given p_T^l bin is thus the average of small $A_{t\bar{t}}$ at low $|Y_{t\bar{t}}|$ with large $A_{t\bar{t}}$ at high $|Y_{t\bar{t}}|$. As p_T^l is increased, the sampling across a range of $Y_{t\bar{t}}$ stays, but the cross section decreases. However, as the change in cross section cancels out in the ratio defining the asymmetry (a normalization effect), $A_{t\bar{t}}$ remains flat.

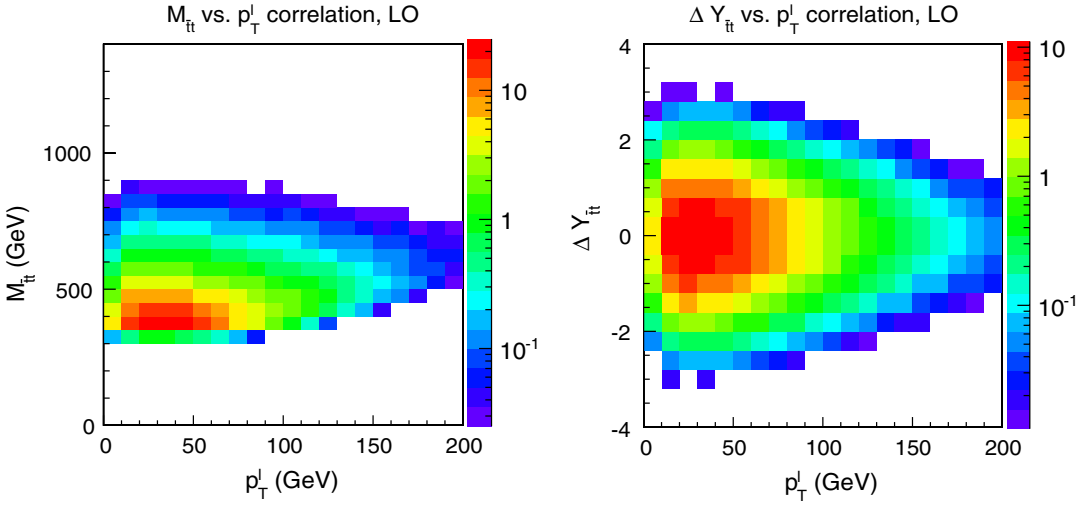

FIG. 3 (color online). The correlation between the lepton p_T and the kinematics of the $t\bar{t}$ system (at LO). The correlation between p_T^l and $m_{t\bar{t}}$ is shown on the left, and the correlation between p_T^l and $\Delta Y_{t\bar{t}}$ is shown on the right.

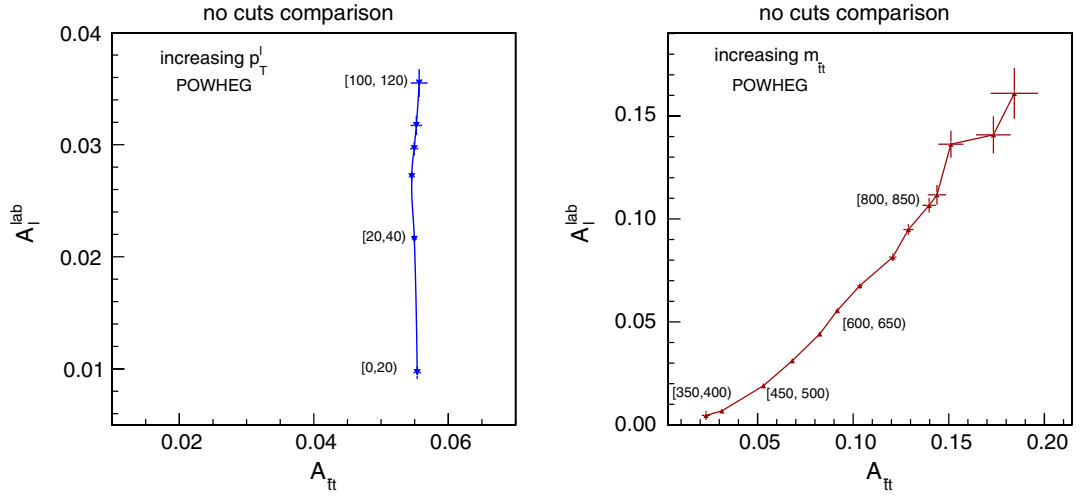

FIG. 4 (color online). The correlation between the leptonic and $t\bar{t}$ asymmetries displayed in the A_l versus $A_{t\bar{t}}$ plane. No cuts have been imposed, and all quantities have been calculated at parton level. In the left panel we show the curve traced out as p_T^l is increased from 0 GeV (bottom point) to 100 GeV (top point) in intervals of 20 GeV—the p_T^l intervals for some of the points are indicated in brackets on the plot. Similarly, in the right panel we present the curve traced out as $m_{t\bar{t}}$ is increased from the threshold value (bottom left) to 1 TeV (top right) in intervals of 50 GeV.

left panel of Fig. 4 corresponds to a different p_T^l bin, which is nothing but the $A_l(p_T^l)[A_{t\bar{t}}(p_T^l)]$ curve mentioned in the introduction. Given the one-dimensional asymmetry spectra explained above, we find that the distribution of points is consistent with a nearly vertical line, and both $A_{t\bar{t}}(p_T^l)$ and $A_l(p_T^l)$ span rather small values. For completeness, we also show, in the right panel of Fig. 4, the asymmetry correlation as a function of $m_{t\bar{t}}$, even though this is not the main focus of this work.

A. Robustness tests

Having understood the interplay between the SM $A_{t\bar{t}}$ and A_l in an idealized scenario, we now study how various effects impact the $A_l(p_T^l) - A_{t\bar{t}}(p_T^l)$ correlations. We continue to work at parton level in this section and will not include cuts. Acceptance cuts and more realistic jet description will be studied in later sections.

The first effect we consider is radiation in decay. The b ($\bar{b}$) from the leptonic top (or antitop) quark can radiate gluons, changing the kinematics and correlations among the top decay products.[6] Radiation in decay will obviously not change the top quark asymmetry, but it may impact how $A_{t\bar{t}}$ is passed on to A_l, e.g., through the analysis

[6]The hadronic W's decay products can also radiate, of course, but since the W is both a color singlet and narrow, this has less influence on the lepton kinematics than the radiation from the lepton's sibling b ($\bar{b}$) quark.

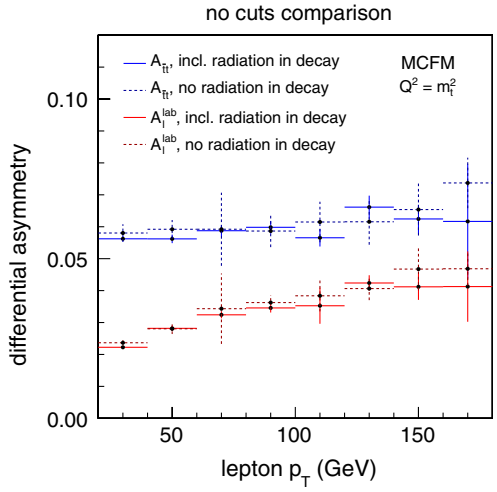

FIG. 5 (color online). A comparison of MCFM results with and without radiation in the top quark decay. The solid line shows the differential distributions $A_{t\bar{t}}(p_T^l)$ and $A_l(p_T^l)$ (lab frame) as a function of the lepton p_T in the most recent version (v6.3), while the dashed line shows the same observable calculated with the previous version. The most recent version includes NLO effects in decays, while the previous iteration contained all decay spin correlations, but no NLO effects in the decays.

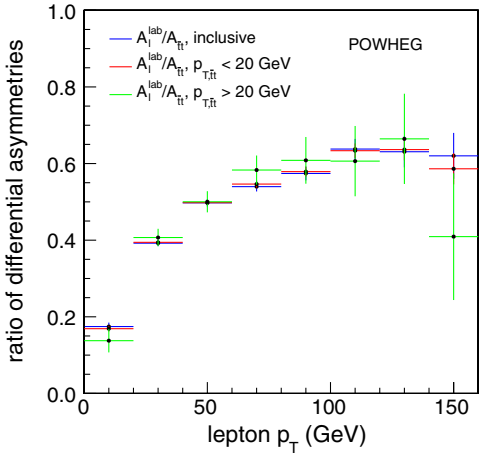

FIG. 6 (color online). The ratio of differential asymmetries $A_l(p_T^l)/A_{t\bar{t}}(p_T^l)$ for different ranges of $p_{T,t\bar{t}}$. The red and green curves show these ratios for events with $p_{T,t\bar{t}} < 20$ GeV and $p_{T,t\bar{t}} > 20$ GeV, respectively. The blue curve is the ratio across all $p_{T,t\bar{t}}$ values. Most of the cross section resides in the lower-$p_{T,t\bar{t}}$ region, so the errors on the high-$p_{T,t\bar{t}}$ region are larger because of limited statistics. All calculations were performed in the idealized SM scenario, at NLO in top quark pair production.

selection cuts. Though radiation in decay occurs at the same order in α_s as the processes that contribute to $A_{t\bar{t}}$, it is further suppressed by the width of the top quark. Recent analytic work on the effects of radiation in decay can be found in Ref. [40], and radiation in decay has been incorporated into the latest version of MCFM [32]. By comparing the study of Fig. 1 between different versions of MCFM, we can study the size of the effect of radiation in decay on our observables, $A_{t\bar{t}}(p_T^l)$ and $A_l(p_T^l)$. As can be seen from Fig. 5, the results with and without radiation in the decay are nearly identical, indicating that the LO treatment of the top quark decay products (but with spin correlations intact) is sufficient to predict the correlation between $A_{t\bar{t}}$ and A_l. As the top quark p_T is ambiguous once radiation in decay is allowed, we perform this cross-check using a fix-scale choice of $Q^2 = m_t^2$.

The second test of robustness concerns the p_T of the $t\bar{t}$ system, $p_{T,t\bar{t}}$. As is well known [3], $A_{t\bar{t}}$ strongly depends on $p_{T,t\bar{t}}$ as it controls the level of real emission in the event. Therefore, among other effects, mismodeling of acceptance cuts or biases in the measurement could lead to a change in the overall normalization of the resulting inclusive and differential value of $A_{t\bar{t}}$. Thus, it is important to verify whether the $A_l - A_{t\bar{t}}$ correlation is sensitive to $p_{T,t\bar{t}}$. Notice that by insisting on large p_T^l, we are forcing the $t\bar{t} + X$ system into the following two possible kinematic configurations: (1) the top and antitop quark move in the same direction, recoiling against hard initial-state radiation, or (2) the top and antitop quark are back to back and both are central. In the first case, large lepton p_T are possible since some of the initial and large $p_{T,t\bar{t}}$ is inherited by the lepton. In the second configuration, the lepton inherits large p_T from the individual top or antitop quark, rather than the $t\bar{t}$ pair. As a result, this configuration is characterized by low $p_{T,t\bar{t}}$, but large $m_{t\bar{t}}$. Given the contributions come from such different kinematic regimes, one may worry that our results in Fig. 1 come from a delicate cancellation between different effects. Any mismodeling of or bias in $p_{T,t\bar{t}}$ would disrupt such a cancellation and destabilize the correlation. One way to see whether a cancellation is occurring is to divide the events into different bins of $p_{T,t\bar{t}}$ and check the $A_l(p_T^l) - A_{t\bar{t}}(p_T^l)$ correlation in each bin. Again, computing $t\bar{t}$ production at NLO, we have performed this test and the results are shown below in Fig. 6. Quantifying the correlation by the ratio $A_l(p_T^l)/A_{t\bar{t}}(p_T^l)$, for $p_{T,t\bar{t}} < 20$ GeV, we see it is the same as the correlation in events with $p_{T,t\bar{t}} > 20$ GeV—a strong indication that the $A_l(p_T^l) - A_{t\bar{t}}(p_T^l)$ correlation does not come from a cancellation of competing effects. Based on our complete NLO analysis, we can therefore conclude it is stable against $p_{T,t\bar{t}}$ mismodeling.

The final avenue we explore within the SM ideal case is scale variation. Because $A_{t\bar{t}}$ vanishes at $\mathcal{O}(\alpha_s^2)$, NLO calculations of differential $t\bar{t}$ properties only result in a leading-order prediction for the asymmetry $A_{t\bar{t}}$. A more accurate determination of the asymmetry would involve understanding $t\bar{t}$, differentially, at NNLO. In the absence of this NNLO calculation (for recent progress on this, see e.g., Refs. [41,42]), one estimate of our ignorance regarding higher-order corrections is to vary the scale used in the $A_{t\bar{t}}$ calculation by a factor of two. While we expect the absolute values of $A_{t\bar{t}}$ and A_l to change as the scale is

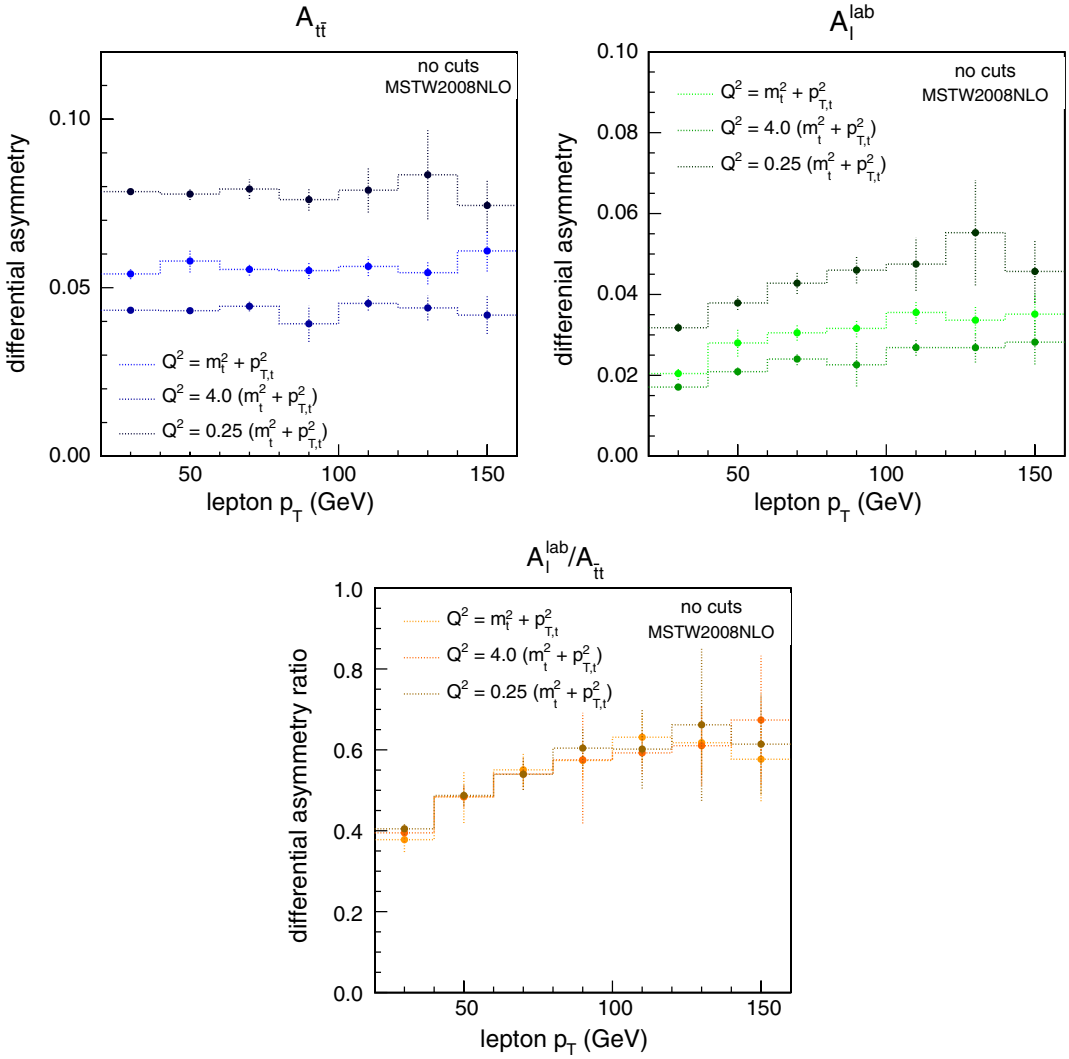

FIG. 7 (color online). Dependence of the asymmetries on the lepton p_T for three different scale choices, calculated using MCFM. The left, middle, and right panel show $A_{t\bar{t}}$, A_l (lab frame) and the ratio $A_l/A_{t\bar{t}}$, respectively. Only the differential asymmetries are depicted, however the same trend is present at the cumulative level, cf. Eqs. (10)–(13). These plots show the ideal SM scenario where no cuts have been applied.

varied, much of the variation is carried in the scale where α_s is evaluated, which cancels out if we take the ratio of asymmetries. A stable ratio $A_l/A_{t\bar{t}}$ under scale variation is therefore a sign that the correlation pointed out here is robust. In Fig. 7 we show the differential distributions $A_{t\bar{t}}(p_T^l)$, $A_l(p_T^l)$ and the ratio $A_l(p_T^l)/A_{t\bar{t}}(p_T^l)$ for the following three different scale choices: $Q^2 = Q_0^2$, $Q^2 = 4 \times Q_0^2$ and $Q^2 = Q_0^2/4$ where $Q_0^2 = m_t^2 + (p_T^t)^2$. The ratio is indeed very stable, as can clearly be seen from the bottom panel of Fig. 7.

III. REALISTIC CASE: SM

We have seen that, in an ideal detector, the lepton and $t\bar{t}$ asymmetries are correlated and follow a robust, predictable curve as a function of the lepton p_T. We must now show to what extent this correlation remains intact in a true hadron collider environment. We proceed in two steps. First, we continue with a parton-level analysis but impose a set of realistic cuts employed by the collaborations in the actual analysis; for concreteness we are going to apply the cuts used by the CDF Collaboration, the ones used by the DØ Collaboration are in practice very similar and have negligible impact on our final conclusions. Second, to further close the gap with the true experimental conditions, we repeat our study including parton shower effects and genuine top quark reconstruction.

A. Parton-level analysis including cuts

Including possible real emission, the parton-level process for $t\bar{t}$ production at NLO has seven final-state particles: one lepton, one neutrino, and up to five jets, two of which originate from b or $\bar{b}$ quarks. Inspired by CDF [7], we impose the following cuts on these objects. We require

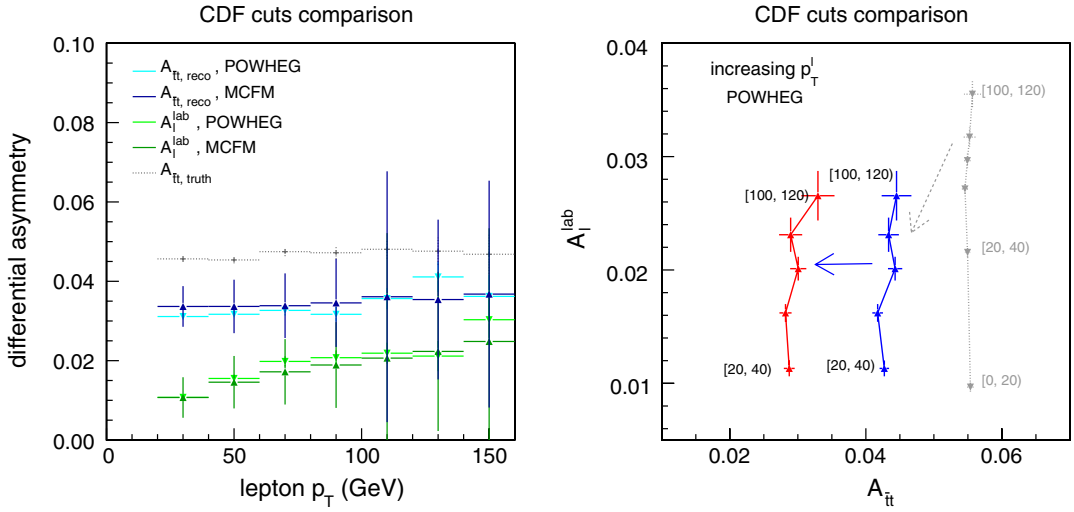

FIG. 8 (color online). Left: differential asymmetries $A_{t\bar{t}}(p_T^l)$ and $A_l(p_T^l)$, where all CDF analysis cuts have been imposed. The darker shaded lines indicate results obtained via MCFM, while the lighter ones show the POWHEG results. Both $A_{t\bar{t}}$ and A_l were calculated in the lab frame, with A_l depicted in green. The blue lines show $A_{t\bar{t}}$ calculated using reconstructed (anti)top quarks, following the scheme in Ref. [32], rather than using the truth information. The grey line shows $A_{t\bar{t}}$ including cuts, but calculated using the true top quark four-vectors rather than using reconstructed objects. Right: the $A_l(p_T^l)[A_{t\bar{t}}(p_T^l)]$ postcuts curve with (red line) and without (blue line) reconstruction compared to the $A_l[A_{t\bar{t}}]$ curve obtained in the ideal case (grey). Because of the lepton cut imposed in the CDF analysis, the new $A_l(p_T^l)[A_{t\bar{t}}(p_T^l)]$ curve starts at 20 GeV rather than zero. The brackets indicate the p_T^l range corresponding to particular points along the $A_l(p_T^l)[A_{t\bar{t}}(p_T^l)]$ curve. The grey arrow indicates how the A_l, $(p_T^l)[A_{t\bar{t}}(p_T^l)]$ curve shifts from cut effects, while the blue arrow shows the effect of reconstruction. Note that only $A_{t\bar{t}}$ is affected by the reconstruction, while both asymmetries are decreased by the analysis cuts.

(i) exactly one lepton of $p_T^l > 20$ GeV and $|\eta^l| < 1.1$.
(ii) $\not{E}_T > 20$ GeV, which we take directly from the p_T of the neutrino.
(iii) jets to have $p_{T,\text{jet}} > 20$ GeV and $|\eta_{\text{jet}}| < 2.0$, and to be formed with the k_T algorithm using a jet size of $R = 0.4$.[7]
(iv) in addition to the above requirements, that all b and $\bar{b}$ jets are restricted to $|\eta^b| < 1.0$. This treatment of bottom quarks means we are effectively tagging both the b and $\bar{b}$ quarks, whereas CDF and DØ only require one tagged jet. This small difference in acceptance may lead to a difference in the absolute values of our calculated asymmetries compared to experiment, but we do not expect it to change our main result.
(v) isolation criteria to be satisfied: $\Delta R_{\text{jet,jet}} > 0.4$ and $\Delta R_{l,\text{jet}} > 0.4$.

Keeping the jet and missing energy cuts fixed to the above, we calculate $A_{t\bar{t}}(p_T^l)$ and $A_l(p_T^l)$, just as we did in the ideal case. As a first step to evaluate this asymmetry, and in particular to evaluate $A_{t\bar{t}}(p_T^l)$, we take the top quark truth information directly from the simulation (no reconstruction). The result is shown in Fig. 8. While the absolute value of the asymmetries is diminished once cuts are imposed (see Fig. 1 for a comparison), the trend in A_l, $A_{t\bar{t}}$ versus p_T^l is preserved.

Another step towards a more realistic analysis is to redo our top quark analysis in terms of reconstructed objects rather than using the truth partonic information (before the decay). While a completely realistic reconstruction will be presented in the next section and will include parton showering effects, we can study some reconstruction effects even at the parton level. Specifically, even at the parton level, jets are sometimes lost due to acceptance or gained from ISR (initial-state radiation), leading to an incorrect reconstruction and a warped $A_{t\bar{t}}$. To study this effect, we compare the $A_{t\bar{t}}$ calculated using perfect top quark reconstruction with the $A_{t\bar{t}}$ calculated using a reconstruction where all five jets, not just those coming from the top quark decays, are considered.[8] This comparison is shown in Fig. 8 as well. The impact it has on $A_{t\bar{t}}$ is sizable, amounting to an $\mathcal{O}(30\%)$ reduction in $A_{t\bar{t}}$. We find that both effects, namely including the acceptance cuts as well as the top quark reconstruction reduce the resulting asymmetries. This is expected since they force the events to be more central, and wrong partonic assignment in realistic reconstruction dilutes the asymmetry.

[7]In the CDF analysis the CDFmidpoint cone algorithm is used, not k_T.

[8]Specifically, we use the "improved" reconstruction introduced in Ref. [32]: all non-b jets are considered in the hadronic W and t reconstruction, and the combination (2 *or* 3 partons) that has invariant mass closest to m_W or m_t is selected.

Finally, we have repeated the scale variation check with the postcut parton-level events and find the same trend as in the ideal cuts case (cf. Fig. 7): while the individual asymmetries $A_{t\bar{t}}(p_T^l)$ and $A_l(p_T^l)$ shift by $\mathcal{O}(25–30\%)$ as the factorization/renormalization scale is varied by a factor of two, the ratio $A_l(p_T^l)/A_{t\bar{t}}(p_T^l)$ remains stable.

B. Showering and reconstruction effects: POWHEG + PYTHIA and SHERPA's CSSHOWER

Having included cuts in our analysis and observed that the correlation between $A_{t\bar{t}}$ and A_l is maintained, the next step towards reality is to include a parton shower. The radiation, which quarks and gluons emit as they lose energy in their evolution from the scale of the hard process to the hadronization scale can show up as additional jets in the detector. This spray of energy, and the combinatorial problem it creates in any analysis relying on reconstruction, tends to dilute parton-level effects. It is therefore important for us to show that our correlation remains visible in the actual environment where the experiments reside.

One way to study the effects of the parton shower on our observable is to pass NLO POWHEG events through PYTHIA [43]. Manipulating the particle-level PYTHIA output into jets via FASTJET [44,45],[9] we can then apply the same analysis cuts as in the previous section. The only subtlety is how we handle b-tagging. In the simple reconstruction used in the last section, we assumed the identity of both b quarks was known, leaving no ambiguity about whether/how to combine the tagged jets with the lepton. In this section, we drop this assumption, choosing to select and reconstruct events exactly as in the CDF analysis [13]. Specifically, provided an event contains a lepton and missing energy passing criteria shown in Sec. III A., the event is kept if it contains four or more jets and at least one b-tag. The leading four jets, one of which must be a b jet, are subsequently divided into a hadronic top quark system and one jet to be paired with the lepton + $\not{E}_T$ system. Each combinatoric possibility in the leptonic W reconstruction and the division of jets is tested, and the combination that best reconstructs the top quark masses (the hadronic and leptonic) is retained. The differential asymmetries for the reconstructed top quarks (and leptons) are shown in Fig. 9, and in the $A_l(p_T^l)[A_{t\bar{t}}(p_T^l)]$ plane on the left panel of Fig. 10. For comparison, we also show $A_{t\bar{t}}(p_T^l)$ and $A_l(p_T^l)$ at parton level.

The experiments typically compare asymmetries at the background-subtracted and unfolded levels, the analog of comparing our fully showered and "ideal scenario" results. However, as we are dealing with Monte Carlo data rather than experimental data, we are able to break down these shifts in multiple stages. Being more quantitative (cf. Fig. 8), we have seen that imposing cuts reduces the leptonic asymmetry by roughly 50% and $A_{t\bar{t}}$ by 20%

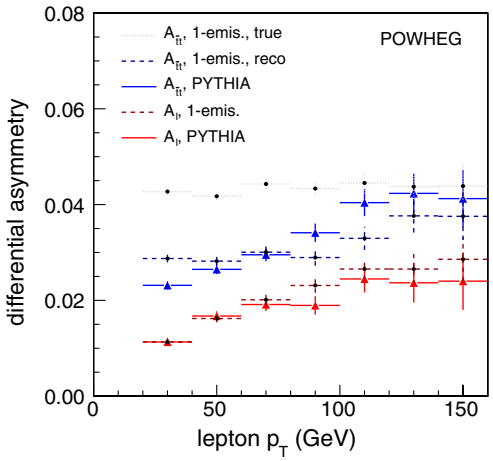

FIG. 9 (color online). Dependence of the differential top quark and lepton asymmetries, versus p_T^l, on parton shower and reconstruction effects. The truth values of $A_{t\bar{t}}(p_T^l)$—after cuts, but without any reconstruction or showering effects—are shown in the uppermost line (grey, dotted). Including reconstruction but staying at parton level, $A_{t\bar{t}}(p_T^l)$ shifts to the dashed blue line. Finally, the postshower, postreconstruction values are given in solid blue. Similarly, the post-PYTHIA, lab frame $A_l(p_T^l)$ is shown by the red solid line, with the red dashed line indicating the lab frame $A_l(p_T^l)$ at parton level.

when compared to the "ideal case" values. Reconstruction does not affect A_l, but it further reduces $A_{t\bar{t}}$ by an additional 30%. Working at the parton level, these reductions are almost independent of the lepton p_T, our proxy for the energy of the $t\bar{t}$ system. Showering and more realistic reconstruction have a p_T^l dependent effect; A_l is shifted by $\mathcal{O}(1–10\%)$, and $A_{t\bar{t}}$ is shifted by $\mathcal{O}(20–30\%)$, with the shifts increasing with p_T^l.

As a second study of the effects of a parton shower on the $A_l - A_{t\bar{t}}$ relationship, we analyze the asymmetry correlation using SHERPA (v1.4.0) [46]. Despite the fact that SHERPA is a LO matrix element generator, the addition of a parton shower technique that appropriately includes color-coherence effects will generate a forward-backward top quark asymmetry (see Ref. [47]), so it is interesting to see to what degree it retains the $A_l - A_{t\bar{t}}$ correlation. To generate events, the LO matrix elements, including the decays of the top quarks, are showered according to SHERPA's color-coherent showering (CSSHOWER) description [48,49]. In the infrared limit of QCD, this description correctly accounts for ISR effects, intermediate top quark radiation and multiple emissions from the final-state b quarks and decay partons.[10] While

[9]We use the k_T algorithm with jet size $R = 0.4$. Jets are identified as b jets if there is a b ($\bar{b}$) parton within the jet area.

[10]For the hard process generation, we use CTEQ6L1 PDFs [50] and an $m_{\perp,t}$-like scale choice ($m_{\perp,t}^2 = m_t^2 + (p_T^t)^2$) resulting from utilizing the default scale setting prescription applied in SHERPA. The top quark decays are incorporated at full matrix element level, i.e., preserving spin correlations and full width effects beyond the narrow-width approximation, with the only requirement of producing intermediate top quark states ($m_t = 173.2$ GeV).

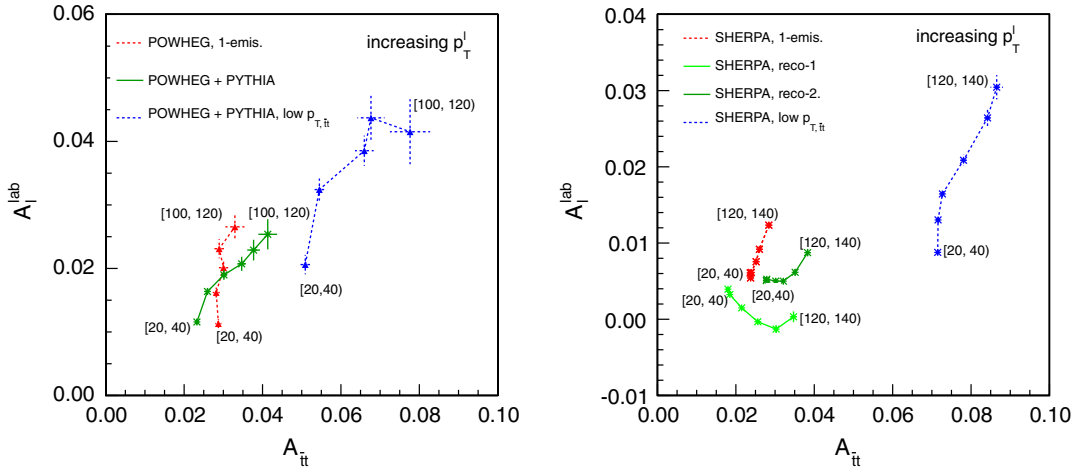

FIG. 10 (color online). Left: the p_T^l dependence of the leptonic and $t\bar{t}$ asymmetries for POWHEG events that have been showered and hadronized with PYTHIA. The postshower $A_l(p_T^l)[A_{t\bar{t}}(p_T^l)]$ curve is shown in dark green and is overlayed on top of the result with cuts and reconstruction done at parton level (red). The blue line shows the postshower result in events where the total $p_{T,t\bar{t}}$ is restricted to $p_{T,t\bar{t}} < 10$ GeV. Right: the analogous curves for events generated with SHERPA's CSSHOWER. The red curve shows $A_l(p_T^l)[A_{t\bar{t}}(p_T^l)]$ with the CSSHOWER truncated at the first emission, the blue curve shows the fully showered result for events restricted to $p_{T,t\bar{t}} < 10$ GeV, and the green curves depict the inclusive, fully showered SHERPA results. The difference between the green curves is the reconstruction algorithm. In the dark green curve, as described in the text, the number of jets included in the reconstruction algorithm is allowed to float, while in the light green curve the number is restricted to four, giving a straightforward, unambiguous reconstruction out of the hardest b and $\bar{b}$ jet and the two leading light-flavor jets. The low-$p_{T,t\bar{t}}$ result uses the latter reconstruction algorithm.

qualitative agreement in $A_{t\bar{t}}$ between the LO matrix element plus parton shower (LO + PS) results and the complete NLO results has been demonstrated [47], exploring $A_l - A_{t\bar{t}}$ tests the adequacy of the LO + PS calculation on a detailed and differential level.

The SHERPA events are reconstructed in similar, but slightly different manner than we used in the POWHEG + PYTHIA case. In particular, the charge of the b jets is assumed to be known, leading to perfect assignment of the b ($\bar{b}$) quarks to the top (antitop) quark.[11] After combining the lepton and missing energy with the correct b jet, the top quark objects are reconstructed by testing *all* possible partitions of jets—even beyond the four jets required for event selection—and keeping the combination which yields the smallest summed-up mass deviation, which we take as $|m^{\text{lep}}_{\text{pseudo-}t} - m_t| + |m^{\text{had}}_{\text{pseudo-}t} - m_t| + \sqrt{2}|m^{\text{had}}_{\text{pseudo-}t,\text{jets}} - m_W|$. By including more jets, the combinatorial issues are bigger for this reconstruction method, however it will capture situations the CDF method cannot, i.e., where the hadronic top quark radiates and manifests itself actually as a four-jet system, or the jet system of the leptonic top quark possesses an extra jet beyond the b jet. The leptonic and $t\bar{t}$ asymmetries derived from the reconstructed SHERPA events are shown in the right panel of Fig. 10. We also show the asymmetries obtained from running SHERPA's CSSHOWER in "one-emission" mode, where showering is terminated after no more than one emission has occurred. The one-emission mode allows us to see the impact of the multiparton emissions and the (enhanced) combinatorial headache coming with them.

Inspecting Fig. 10, while the shapes of the differential asymmetry curves at parton (or one-emission) level agree reasonably, the results after the full shower are quite different. The slope of the POWHEG + PYTHIA curve acquires a slight tilt, as the later/secondary shower emissions drive the slope of $A_{t\bar{t}}(p_T^l)$ and $A_l(p_T^l)$ slightly in opposite directions (see Fig. 9). For the SHERPA result, higher/secondary emissions drive $A_{t\bar{t}}$ and A_l in the same directions as POWHEG + PYTHIA (the A_l is slightly drecreased, while the $A_{t\bar{t}}$ is enhanced,[12] especially at high p_T^l), however the change in slope is much more dramatic: A_l is decreased nearly to zero, or even negative, until $p_T^l \gtrsim 100$ GeV. Massaging the SHERPA top reconstruction algorithm does not fix the discrepancy—the simplified reconstruction used in the lower curve of the SHERPA panel in Fig. 10 is closer to the method used for POWHEG, yet the $A_l(p_T^l)[A_{t\bar{t}}(p_T^l)]$ curve is just as disparate.

The low-$p_{T,t\bar{t}}$ curves in Fig. 10 offer some insight into why the postshower results disagree. The transverse momentum of the $t\bar{t}$ system separates the so-called "Sudakov region"—where $A_{t\bar{t}}$ is positive—from the "hard-p_T region," where the entire $t\bar{t}$ system recoils against additional radiation and the asymmetry is negative. By imposing a low cut on $p_{T,t\bar{t}}$ we can focus on the effects

[11]We obtain this information from a k_T jet algorithm where we systematically keep track of the b-parton flavors.

[12]A larger enhancement from SHERPA's CSSHOWER is expected [47] because subsequent emissions in the shower are still carried out in a color-coherent manner.

that drive the positive asymmetry and are generated by the virtual corrections and multiple soft gluon emission. The majority of the cross section resides in this low-p_T region, so it is important to understand and study the asymmetry here. As we can see, the low $p_{T,t\bar{t}}$ curves closely follow the ideal NLO case (cf. the discussion in Sec. II), despite the fact that all virtual pieces beyond the soft and collinear approximation, i.e., beyond the lowest order Sudakov description are absent in the SHERPA CSSHOWER description. In other words, for regions of phase space close to Born kinematics, the LO + PS and NLO calculations are in relative agreement. Note that the denominator in the SHERPA asymmetry calculation is the lowest order cross section and is smaller than the NLO cross section used for POWHEG.

However, turning to the inclusive case, the calculation becomes sensitive to the whole $p_{T,t\bar{t}}$ region and how it is modeled. As discussed in Ref. [47], in color-coherent parton showers like the CSSHOWER, the real-emission effect is overestimated because leading-N_C color factors, rather than the smaller, NLO-correct factors, are utilized and the use of the eikonal limit/dipole radiation functions is extended beyond its/their reliable range. The enhanced emission leads to a stronger reduction of the already smaller virtual effects as soon as we go away from the low $p_{T,t\bar{t}}$ limit. The shower Sudakov effect (the enhanced asymmetry in the low-$p_{T,t\bar{t}}$ region) is weaker than the enhancement in the full NLO calculation, so the negative contributions from emission win out and drag the asymmetries down. So, although the SHERPA CSSHOWER qualitatively generates an $A_{t\bar{t}}(p_{T,t\bar{t}})$ similarly to POWHEG + PYTHIA, it cannot reproduce it in the details, and the details are important to get the $A_l(p_T^l)[A_{t\bar{t}}(p_T^l)]$ correlation right. One reason the lepton asymmetry may be more sensitive to the shower details may be the tight rapidity cut, $|\eta^l| < 1.1$, whereas $|\eta_{\text{jet}}| < 2.0$. Being so central, the leptons can easily be nudged from forwards-moving to backwards-moving (or vice versa) or driven out of (into) the acceptance range, making A_l more susceptible to later shower emissions. We emphasize that the instability shown in Fig. 10 is not SHERPA-specific, any LO + PS calculator will struggle to capture the details of the $A_l(p_T^l)[A_{t\bar{t}}(p_T^l)]$ correlation for the reasons mentioned above.

To summarize, we find that the qualitative features of the SM $A_{t\bar{t}}(p_T^l) - A_l(p_T^l)$ correlation are maintained throughout all levels of event and analysis complexity. The absolute values of the asymmetries and their relation to each other do shift depending on the stage of the analysis, but the slope of the $A_l(p_T^l)[A_{t\bar{t}}(p_T^l)]$ curve is maintained. Importantly, to see the robustness of this result, one *must* use calculational tools that are exact at NLO (such as POWHEG + PYTHIA). Lowest order matrix element calculators supplemented with a parton shower respecting color coherence may be sufficient to describe gross features of $A_{t\bar{t}}$ and do offer valuable insight to the physics behind the asymmetry, but these tools lack some of the physics necessary to capture detailed effects like the correlation between differential asymmetries. While the sensitivity of differential correlations shown here should serve as a warning label on calculations done with LO + PS accuracy, as we will show in detail in the next section, the $A_l(p_T^l)[A_{t\bar{t}}(p_T^l)]$ curves in various benchmark BSM scenarios are dramatically different from the SM curve. Therefore, small shifts (in absolute value) in the asymmetries originating from cut, reconstruction or shower effects will not seriously hinder the discriminating power of the $A_l(p_T^l)[A_{t\bar{t}}(p_T^l)]$ correlation.

IV. ASYMMETRIES BEYOND THE STANDARD MODEL

As we have discussed, in the SM the shape of $A_l(p_T^l)[A_{t\bar{t}}(p_T^l)]$ can be simply understood as a consequence of the fact that $t\bar{t}$ production in QCD is unpolarized. In particular, the same number of left- and right-handed top quarks is produced, and that equal amounts of $t\bar{t}$ pairs are produced in collisions of left- and right-handed quarks. The latter fact ensures that the lepton asymmetry vanishes at the $t\bar{t}$ production threshold [30]. On the other hand, the fact that the top quarks have no overall polarization ensures that, for top quarks produced with a significant momentum, the lepton direction is determined by the kinematics of the boosted top quark decay. These simple arguments explain the behavior of $A_l(p_T^l)/A_{t\bar{t}}(p_T^l)$ in the SM. At small p_T^l the lepton asymmetry is dominated by the near-threshold sample, and one expects $A_l(p_T^l) \ll A_{t\bar{t}}(p_T^l)$. As p_T^l grows the lepton direction becomes more and more correlated with that of the parent top quark, therefore one expects $A_l(p_T^l)$ to approach the $A_{t\bar{t}}(p_T^l)$ curve from below. This is indeed what comes out of the MC simulations we presented in Secs. II and III. Moreover, we found that the top quark asymmetry is approximately independent of p_T^l due to an interplay between two effects: the increase of $A_{t\bar{t}}$ as a function of $m_{t\bar{t}}$ (correlated with p_T^l) and the increase of $A_{t\bar{t}}$ as a function of $\Delta Y_{t\bar{t}}$ (anticorrelated with p_T^l).

These expectations can be grossly violated in models beyond the SM. New physics may introduce two effects that could potentially distort the shape of $A_l(p_T^l)[A_{t\bar{t}}(p_T^l)]$ away from the SM prediction. One is that BSM models addressing the anomalous $t\bar{t}$ asymmetry at the Tevatron may lead to a very different $m_{t\bar{t}}$ dependence of the asymmetry. Because of the correlation between p_T^l and $m_{t\bar{t}}$, in the presence of new physics there is no reason for $A_{t\bar{t}}(p_T^l)$ to remain approximately constant as in the SM. In fact, as we will see below, $A_{t\bar{t}}(p_T^l)$ can either increase or decrease, and the strength of the effect is strongly model dependent. The other important effect is polarization. Models addressing the anomalous top quark asymmetry measured at the Tevatron introduce new particles with different couplings to left- and right-handed quarks. This typically leads to polarization both in production and in the final state. These polarization effects may be observable, as pointed out many times in the literature [25,28,29,51–54]. In particular, the inclusive [26]

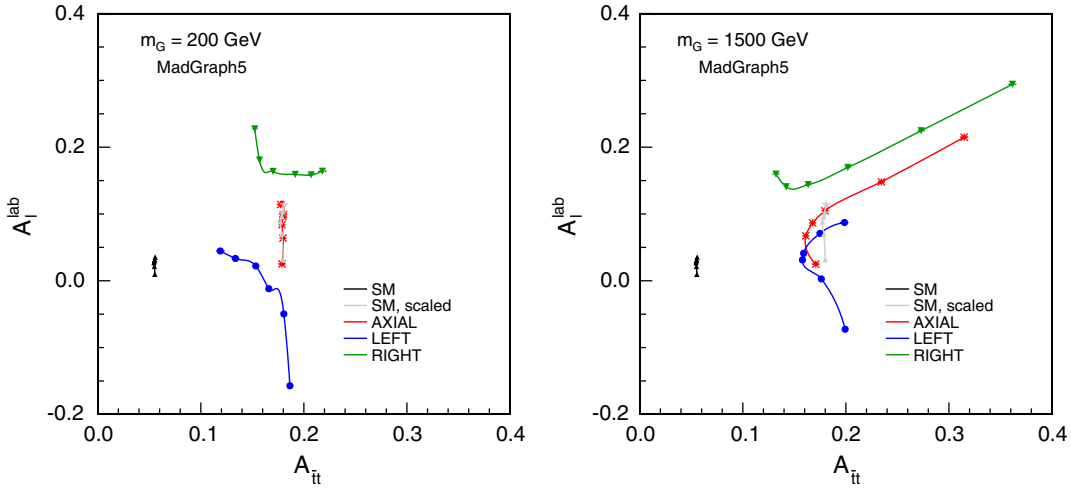

FIG. 11 (color online). Left: the $A_l(p_T^l)[A_{t\bar{t}}(p_T^l)]$ curves for increasing p_T^l bins in the axigluon benchmarks with $m_G = 200$ GeV with left-handed (blue), right-handed (green), and axial (red) couplings, as specified in Eq. (15). Also shown here, analogous SM curve (black) for comparison, and a "rescaled SM" curve (grey), where $A_{t\bar{t}}$ has been artificially inflated to 0.18—the current experimental value. This rescaled curve emphasizes the difference in slope between the SM and our benchmark BSM scenarios. Right: the same curves presented for the axigluon benchmarks with $m_G = 1.5$ TeV as specified in Eq. (16).

and threshold [30] lepton asymmetries are important observables to test the SM and discriminate between different models of new physics predicting the same top quark asymmetry. Here we point out that studying the p_T^l dependence of $A_{t\bar{t}}(p_T^l)$ and $A_l(p_T^l)$ provides further discriminating power.

To illustrate it, we study $A_{t\bar{t}}(p_T^l)$ and $A_l(p_T^l)$ in BSM models that lead to an enhanced top quark asymmetry in agreement with the Tevatron observations. We focus on the so-called s-channel axigluon. In this model one introduces a color-octet field G_μ^a with mass m_G and the couplings to quarks that are assumed to be flavor diagonal but otherwise arbitrary:

$$\mathcal{L} \subset g_{L,i}\bar{q}_i\bar{\sigma}^\mu G_\mu^a T^a q_i + g_{R,i}q_i^c\sigma^\mu G_\mu^a T^a \bar{q}_i^c, \quad (14)$$

where q_i and q_i^c denote left-handed doublet and right-handed singlet quarks, respectively. If the axigluon couplings to the top and light quarks are chiral, $g_L \neq g_R$, then interference of the s-channel axigluon exchange with the tree-level QCD gluon exchange results in a non-zero forward-backward asymmetry of the $q\bar{q} \to t\bar{t}$ production process. There exist regions in the parameter space of the axigluon mass and couplings leading to an $\mathcal{O}(10\%)$ additional contribution to the inclusive top quark asymmetry, bringing the theoretical prediction to a good agreement with the central value observed by CDF and DØ, while keeping the total $t\bar{t}$ cross section within the experimental bounds. To avoid the bounds from dijet production and $t\bar{t}$ resonance searches, the axigluon should have a significant width, $\Gamma_G \gtrsim 0.2 m_G$.

In the following we study in detail the predictions concerning $A_{t\bar{t}}(p_T^l)$ and $A_l(p_T^l)$ for a representative set of axigluon benchmark models. One class has a relatively light and wide axigluon, $m_G = 200$ GeV, $\Gamma_G = 50$ GeV, with flavor universal couplings to the SM quarks. For this mass, we pick three benchmarks with left-handed, right-handed, and axial axigluon couplings to the quarks, each predicting the same $\Delta A_{t\bar{t}} = 0.12$ contribution to the inclusive top quark asymmetry—on top of the SM contribution of $\mathcal{O}(9\%)$—but each predicting a different lepton asymmetry. The couplings, the axigluon width, and the computed lepton asymmetries take the following values:

$$\begin{aligned}
&\text{(L)}\ g_{R,i} = 0,\ g_{L,i} = 0.8 g_s\text{: } \Delta A_l = -0.07,\\
&\text{(R)}\ g_{R,i} = 0.8 g_s,\ g_{L,i} = 0\text{: } \Delta A_l = 0.18,\\
&\text{(A)}\ g_{R,i} = 0.4 g_s,\ g_{L,i} = -0.4 g_s\text{: } \Delta A_l = 0.05,
\end{aligned} \quad (15)$$

where g_s is the QCD coupling. For those benchmarks, the axigluon decay width into $q\bar{q}$ pairs is of order one GeV, thus the larger width we assumed must be explained by exotic decay channels (see e.g., Ref. [55]).

The other class of benchmarks has a relatively heavy axigluon, $m_G = 1.5$ TeV, and flavor nonuniversal couplings (see Refs. [56–66] for some theoretical constructions of heavy axigluon models). Again we pick three benchmarks with left-handed, right-handed, and axial axigluon couplings:

$$\begin{aligned}
&\text{(L)}\ g_{L,q} = -1.3 g_s,\ g_{R,q} = 0,\ g_{L,t} = 6 g_s,\ g_{R,t} = 0\text{: } \Delta A_l = -0.01,\ \Gamma_G = 970\ \text{GeV},\\
&\text{(R)}\ g_{L,q} = 0,\ g_{R,q} = -1.1 g_s,\ g_{L,t} = 0,\ g_{R,t} = 6 g_s\text{: } \Delta A_l = 0.14,\ \Gamma_G = 460\ \text{GeV}\\
&\text{(A)}\ g_{L,q} = 0.6 g_s,\ g_{R,q} = -0.6 g_s,\ g_{L,t} = -3 g_s,\ g_{R,t} = 3 g_s\text{: } \Delta A_l = 0.06,\ \Gamma_G = 350\ \text{GeV},
\end{aligned} \quad (16)$$

where above q stands for doublet and up-type singlet quarks of the first and the second generation (the couplings to down-type singlet quarks are assumed to vanish). In this case the axigluon width is assumed to be dominated by two-body decays into the SM quarks, as follows from the coupling values listed above. As for the light axigluon models, each of the benchmarks in Eq. (16) predicts $\Delta A_{t\bar{t}} = 0.12$.

In Fig. 11, we plot the p_T^l dependence of the top quark and lepton asymmetries. To compute the asymmetries, we simulated semileptonically decaying $t\bar{t}$ events using MADGRAPH 5 [67] with a custom user-defined model describing the extension of the SM with the axigluon coupled to quarks as in Eq. (14). The asymmetries were computed using the parton-level input without taking into account showering, hadronization, detector, or reconstruction effects. The samples were divided according to p_T^l into six bins with the lower bin limits at 0, 20, 40, 60, 100, 150 GeV, and the points in Fig. 11 refer to the asymmetries in these bins. As our simulations are given at tree level and do not include the one-loop SM contribution, we simply add to the results in each bin the SM asymmetries in that bin estimated by POWHEG.[13]

As can be seen in Fig. 11, the differences between the benchmarks become more pronounced when the p_T^l dependence is exploited. The striking observation is that the slope of the curve traced in the $A_{t\bar{t}}$-A_ℓ plane can be completely different than in the SM. For the light axigluon case, the (R) benchmark predicts an approximately constant $A_l(p_T^l)$ and increasing $A_{t\bar{t}}(p_T^l)$, while for the (L) benchmark $A_l(p_T^l)$ is increasing and $A_{t\bar{t}}(p_T^l)$ is decreasing. In both of these cases the shape of the curve can be qualitatively understood. At low p_T^l the lepton asymmetry is close to its thresholds value and approaches $A_{t\bar{t}}(p_T^l)$ at large p_T^l. The shape of $A_{t\bar{t}}(p_T^l)$ is influenced by the top quark polarization: in the (L/R) case boosted top quarks have dominantly left/right helicity and tend to emit the lepton in the opposite/same direction as the top quark. For low and moderate p_T^l, this leads to a certain degree of anti-correlation/correlation with $m_{t\bar{t}}$, and the derivative of $A_{t\bar{t}}(p_T^l)$ reflects the increasing $t\bar{t}$ asymmetry as function of $m_{t\bar{t}}$. On the other hand the (A) benchmark, where polarization effects are small and completely vanishing at the $t\bar{t}$ threshold, predicts the shape $A_{t\bar{t}}(p_T^l)$ and $A_l(p_T^l)$ similarly to the SM, except that both lepton and top quark asymmetries in each bin are shifted to larger values.

Very similar arguments hold for the heavy axigluon benchmarks. One important difference between light and heavy axigluon benchmarks is that the latter predict a much steeper dependence of the top quark asymmetry on $m_{t\bar{t}}$. This is the reason why the p_T^l dependence is more pronounced for the heavy axigluon benchmarks. In particular, $A_{t\bar{t}}(p_T^l)$ steeply grows at high p_T^l as a result of the correlation between p_T^l and $m_{t\bar{t}}$. For the (L) benchmark this leads to a "turnaround" of the curve when the anticorrelation between p_T^l and $m_{t\bar{t}}$ at low p_T^l owing to the top quark polarization turns into correlation at high values of p_T^l.

In summary, the p_T^l dependence of the lepton and top quark asymmetries offers a handle to discriminate between the SM and new physics, and also between different models of new physics predicting the same top quark asymmetry. This test of the SM is to a large extent independent of the overall normalization of the asymmetries. If, hypothetically, some yet uncalculated higher-order QCD corrections to the asymmetries happen to be much larger than expected, they may shift the curve in the $A_l(p_T^l) - A_{t\bar{t}}(p_T^l)$ to higher values without changing its shape. On the other hand, the shape of the curve in the $A_l - A_{t\bar{t}}$ plane is very sensitive to polarization effects, which typically are present in BSM models addressing the anomalous top quark asymmetry at the Tevatron.

V. DISCUSSION: ADDITIONAL RECONSTRUCTION-INDEPENDENT QUANTITIES

Throughout this paper we have used p_T^l to study the relation between A_l and $A_{t\bar{t}}$ in various kinematic regimes. The lepton p_T is a useful variable to consider as a probe since it is simple, clean, and—just like A_l—it does not require reconstruction of any complicated objects. However, it is not the only option. Along with the properties of the lepton, there are several global observables, such as the total invariant mass taken over all visible final-state objects, $m_{\rm vis}$, that are also reconstruction independent. A few other examples are H_T, m_T, and $m_{T,\rm vis}$. Here, H_T is defined in the usual way as the scalar sum H_T of all identified-object p_T including $\not{E}_T$; similarly, combining all leptons and jets in the event (even beyond those required for selection) into a single "visible" four-vector, $p_{\rm vis}$, the other transverse quantities are given as (cf. Ref. [68])

$$m_T^2 = \left(\sum_{i=l,\rm jet} |\vec{p}_{T,i}| + |\not{E}_T|\right)^2 - (\vec{p}_{T,\rm vis} + \vec{\not{E}}_T)^2,$$
$$m_{T,\rm vis}^2 = m_{\rm vis}^2 + 2(E_{T,\rm vis}|\not{E}_T| - \vec{p}_{T,\rm vis}\cdot\vec{\not{E}}_T), \quad (17)$$

where

$$m_{\rm vis}^2 = p_{\rm vis}^2, \quad \vec{p}_{T,\rm vis} = \sum_{i=l,\rm jet}\vec{p}_{T,i}, \quad E_{T,\rm vis}^2 = m_{\rm vis}^2 + p_{T,\rm vis}^2 \quad (18)$$

denote the mass, transverse momentum, and transverse energy of the visible system.

Studies using reconstruction-independent asymmetries and/or variables such as these are useful for a couple of reasons. First, reconstruction-independent quantities have

[13]Both the SM and BSM asymmetries are dominated by the interference of the tree-level QCD amplitude with the one-loop amplitude in the former case, and with the tree-level s-channel axigluon exchange in the latter, so it is reasonable to assume that the two effects add up.

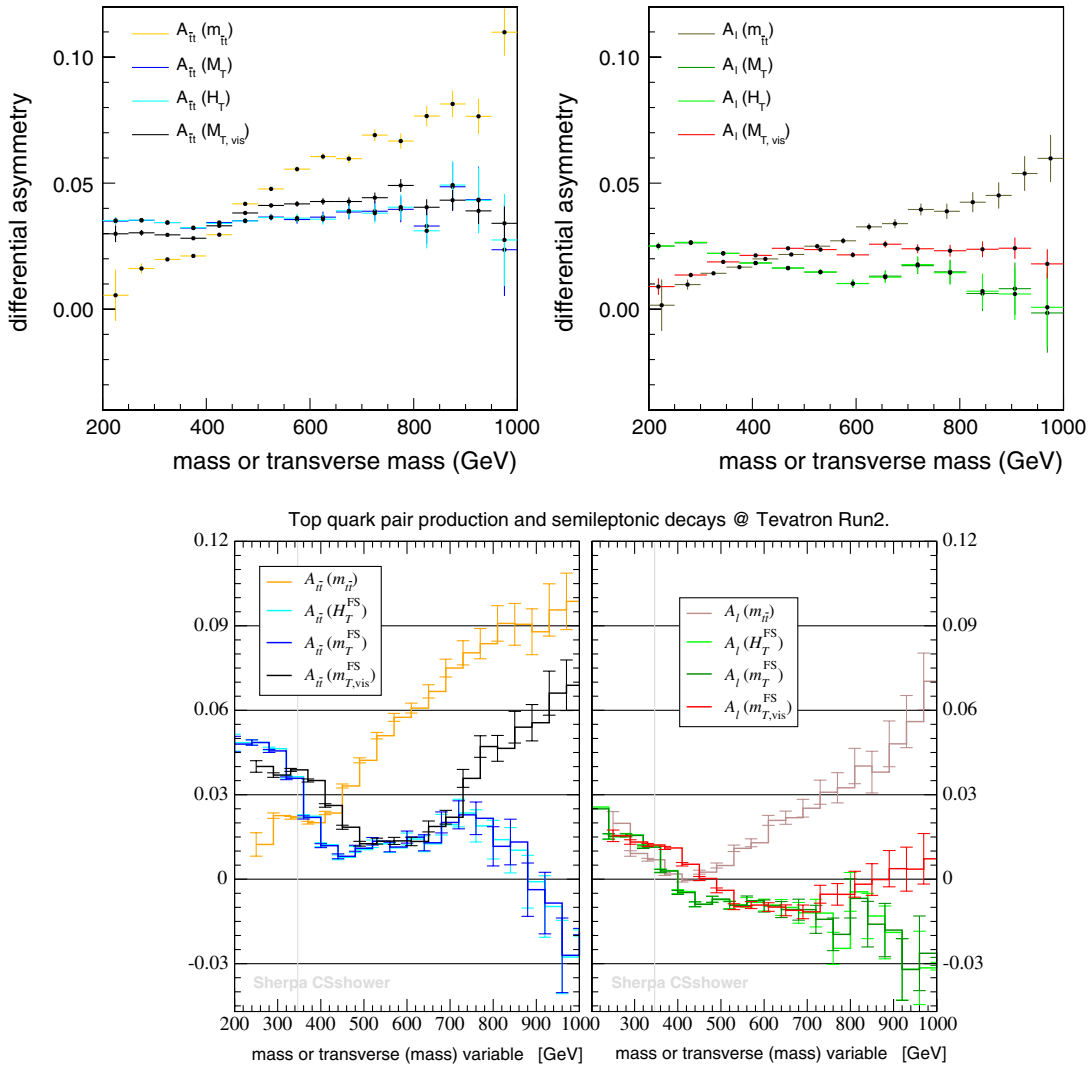

FIG. 12 (color online). Differential forward-backward (left) and lepton-based asymmetries (right) in $t\bar{t}$ events as a function of various transverse observables (and for comparison, as a function of $m_{t\bar{t}}$) using CDF-like event selection (see Sec. III A). The results in the top two panels were obtained by running POWHEG + PYTHIA, while the bottom panels show results from SHERPA (all generated as in Sec. III B).

no (intrinsic) combinatorial issues, so the sensitivity to how these objects are chosen is significantly reduced. Second, as they are inclusive, these quantities are less sensitive to the modeling of the various distributions involved in the actual measurements. As a result, systematic uncertainties are under better control. Third, we can introduce additional analysis levels with varying degree of reconstruction dependence (e.g., reconstruction-dependent asymmetry, $A_{t\bar{t}}$, versus reconstruction-independent observable, m_T), allowing for a number of sanity and closure tests on the existing data. For example, if the Tevatron Collaborations were to measure the dependence of the asymmetries on one of the variables introduced above and find agreement with our studies, that would strongly hint at an error in the reconstruction. With no more data-taking at the Tevatron, it is essential to try out each different angle in forming differential asymmetry measurements as it might be the only way to shed more light on the present data versus theory puzzle.

To illustrate this in more detail, we present in Fig. 12 the differential top quark (left panels) and lepton (right panels) asymmetries with respect to the final-state variables discussed above. These events were generated using POWHEG + PYTHIA (top panels), and simultaneously with SHERPA (bottom panels) following the same procedure as in Sec. III B. For comparison, we also show the differential asymmetries with respect to $m_{t\bar{t}}$. The qualitative similarity between results in the different generators is evidence for the decreased modeling sensitivity mentioned above.

Focusing on $A_{t\bar{t}}$, the asymmetry with respect to H_T does not rise nearly as fast as $A_{t\bar{t}}(m_{t\bar{t}})$. This occurs because H_T is sensitive to extra radiation in the event, while $m_{t\bar{t}}$ is not.

Events that have large H_T due to lots of extra radiation will carry a large, negative asymmetry, partially counteracting the large positive asymmetry generated by large $m_{t\bar{t}}$, large H_T events. Similarly, the design of the selection cuts is such that in most cases the visible transverse momentum is balanced out by the missing transverse energy vector. This yields an asymmetry dependence on m_T that is very close to that of H_T. Finally, we use $m_{T,\mathrm{vis}}$ rather than m_{vis} alone, because $m_{T,\mathrm{vis}}$ contains some missing energy information and thereby gives a better approximation to the total invariant mass of the $t\bar{t}+X$ system. The effect only kicks in for larger transverse masses where $A_{t\bar{t}}(m_{T,\mathrm{vis}})$ starts to follow the $m_{t\bar{t}}$ dependence of $A_{t\bar{t}}$. In the low $m_{T,\mathrm{vis}}$ region the transverse character of the observable still dominates, leading to an H_T-like asymmetry dependence.

Turning to the dependence of A_l, we find that the differential leptonic asymmetry actually is quite insensitive to the choice of the specific transverse variables and is very small in magnitude ($|A_l(x)| \leq 2\%$), potentially too small to be observed at the Tevatron (even without requiring top quark reconstruction). However, this argument can be turned around in the sense that the standard model gives predictions that by and large are ''consistent with zero.'' Hence any measurement deviating from zero in these observables can be considered as a fairly clear signal for new physics.

It is interesting to explore these ''reconstruction-free'' distributions both from an experimental point of view as well as from the theoretical perspective, where one should study the robustness of this new set of observables more carefully. Such a semi-inclusive approach can, in principle, lead to a cleaner set of precision observables and, in the future, also turn out to be useful for the LHC experiments.

VI. CONCLUSIONS

The $t\bar{t}$ asymmetry measured by the CDF and DØ Collaborations remains higher than expected in the standard model (SM), both when measured inclusively and when binned in kinematic variables such as $m_{t\bar{t}}$ or $Y_{t\bar{t}}$. In order to determine the origin of the discrepancy, in this paper we have proposed that the leptonic asymmetry A_l is a useful probe. Within the SM, A_l is inherited from $A_{t\bar{t}}$, with the relationship between the two set by the kinematics of the $t\bar{t}$ system. Thus, by varying the lepton p_T—a simple proxy for the mother-top quark energy, directionality and spin—one obtains a simple correlation between the top quark and lepton-based asymmetries which can be conveniently described by a curve $A_l[A_{t\bar{t}}(p_T^l)]$ in the $A_l - A_{t\bar{t}}$ plane. We have verified that this correlation between asymmetries is qualitatively maintained through all levels of the analysis, from parton level through the inclusion of showering and reconstruction. The correlation is also stable under variations of theory inputs and under potential mismodeling.

By studying the full $A_l - A_{t\bar{t}}$ correlation in data (and their individual p_T^l dependence), rather than just the inclusive asymmetries, we gain discriminating power. The slope of the curve is insensitive to the size of the overall normalization of the asymmetry and is found to be rather stable against various deformation of inputs and analysis parameters. The slope is, however, not satisfactorily modeled by LO + PS tools and requires complete NLO (+ PS) treatment. We have demonstrated the discriminating power of the $A_l(p_T^l)[A_{t\bar{t}}(p_T^l)]$ correlation by showing several beyond the SM benchmarks with the same net asymmetry but with correlations in the $A_l - A_{t\bar{t}}$ plane that are all distinct and distinct from the SM case. This argument for studying the correlation among asymmetries is not unique to the semileptonic $t\bar{t}$ channel, nor is it unique to the Tevatron. It is important to keep in mind that, even if the central values of observables such as A_C at the LHC turn out to match the SM values within uncertainties, the correlation of A_C with other asymmetries in the $t\bar{t}$ system are a worthwhile test of the SM, and can be proven to be more stable similar to the case discussed above. We have also briefly considered how the asymmetry can be measured via more inclusive, reconstruction-free variables. These can be further used in principle to control the measurement of top quark precision observables and might provide us with extra sensitivity to the presence of non-standard model contributions to the various asymmetries.

ACKNOWLEDGMENTS

We are thankful to Dan Amidei, Keith Hamilton, Amnon Harel, Stefan Höche, Paolo Nason, Gavin Salam, Michael Trott, and Ciaran Williams for many helpful discussions. G. P. is the Shlomo and Michla Tomarin development chair, supported by grants from GIF, Gruber Foundation, IRG, ISF, and Minerva.

[1] J. H. Kuhn and G. Rodrigo, Phys. Rev. Lett. **81**, 49 (1998).
[2] J. H. Kuhn and G. Rodrigo, Phys. Rev. D **59**, 054017 (1999).
[3] M. Bowen, S. Ellis, and D. Rainwater, Phys. Rev. D **73**, 014008 (2006).
[4] O. Antunano, J. H. Kuhn, and G. Rodrigo, Phys. Rev. D **77**, 014003 (2008).
[5] L. G. Almeida, G. F. Sterman, and W. Vogelsang, Phys. Rev. D **78**, 014008 (2008).
[6] T. Aaltonen *et al.* (CDF Collaboration), arXiv:1211.1003.

[7] T. Aaltonen *et al.* (CDF Collaboration), Phys. Rev. D **83**, 112003 (2011).
[8] V. M. Abazov *et al.* (DØ Collaboration), Phys. Rev. D **84**, 112005 (2011).
[9] W. Hollik and D. Pagani, Phys. Rev. D **84**, 093003 (2011).
[10] A. V. Manohar and M. Trott, Phys. Lett. B **711**, 313 (2012).
[11] W. Bernreuther and Z.-G. Si, Phys. Rev. D **86**, 034026 (2012).
[12] J. Drobnak, A. L. Kagan, J. F. Kamenik, G. Perez, and J. Zupan, arXiv:1209.4872.
[13] T. Aaltonen *et al.* (CDF Collaboration), CDF note Report No. 10807, 2012.
[14] T. Aaltonen *et al.* (CDF Collaboration), CDF note Report No. 10436, 2011.
[15] V. M. Abazov *et al.* (DØ Collaboration), arXiv:1207.0364.
[16] ATLAS Collaboration, CERN, Technical Report No ATLAS-CONF-2012-057, 2012.
[17] S. Chatrchyan *et al.* (CMS Collaboration), Phys. Lett. B **717**, 129 (2012).
[18] S. Chatrchyan *et al.* (CMS Collaboration), Phys. Lett. B **709**, 28 (2012).
[19] J. Aguilar-Saavedra and A. Juste, Phys. Rev. Lett. **109**, 211804 (2012).
[20] E. Alvarez and E. C. Leskow, Phys. Rev. D **86**, 114034 (2012).
[21] J. Drobnak, J. F. Kamenik, and J. Zupan, arXiv:1205.4721.
[22] J. F. Kamenik, J. Shu, and J. Zupan, Eur. Phys. J. C **72**, 2012 (2012).
[23] K. Agashe, A. Belyaev, T. Krupovnickas, G. Perez, and J. Virzi, Phys. Rev. D **77**, 015003 (2008).
[24] L. G. Almeida, S. J. Lee, G. Perez, I. Sung, and J. Virzi, Phys. Rev. D **79**, 074012 (2009).
[25] D. Choudhury, R. M. Godbole, S. D. Rindani, and P. Saha, Phys. Rev. D **84**, 014023 (2011).
[26] D. Krohn, T. Liu, J. Shelton, and L.-T. Wang, Phys. Rev. D **84**, 074034 (2011).
[27] E. L. Berger, Q.-H. Cao, C.-R. Chen, J.-H. Yu, and H. Zhang, Phys. Rev. Lett. **108**, 072002 (2012).
[28] E. L. Berger, Q.-H. Cao, C.-R. Chen, and H. Zhang, arXiv:1209.4899.
[29] J. Cao, L. Wu, and J. M. Yang, Phys. Rev. D **83**, 034024 (2011).
[30] A. Falkowski, G. Perez, and M. Schmaltz, arXiv:1110.3796.
[31] J. M. Campbell, R. K. Ellis, and C. Williams, J. High Energy Phys. 07 (2011) 018.
[32] J. M. Campbell and R. K. Ellis, arXiv:1204.1513.
[33] P. Nason, J. High Energy Phys. 11 (2004) 040.
[34] S. Frixione, P. Nason, and C. Oleari, J. High Energy Phys. 11 (2007) 070.
[35] S. Alioli, P. Nason, C. Oleari, and E. Re, J. High Energy Phys. 06 (2010) 043.
[36] S. Frixione, P. Nason, and G. Ridolfi, J. High Energy Phys. 09 (2007) 126.
[37] A. Martin, W. Stirling, R. Thorne, and G. Watt, Eur. Phys. J. C **63**, 189 (2009).
[38] V. Ahrens, A. Ferroglia, M. Neubert, B. D. Pecjak, and L. L. Yang, Phys. Rev. D **84**, 074004 (2011).
[39] N. Kidonakis and B. D. Pecjak, Eur. Phys. J. C **72**, 2084 (2012).
[40] K. Melnikov, A. Scharf, and M. Schulze, Phys. Rev. D **85**, 054002 (2012).
[41] P. Bärnreuther, M. Czakon, and A. Mitov, Phys. Rev. Lett. **109**, 132001 (2012).
[42] M. Czakon and A. Mitov, J. High Energy Phys. 01 (2013) 080.
[43] T. Sjostrand, S. Mrenna, and P. Z. Skands, Comput. Phys. Commun. **178**, 852 (2008).
[44] M. Cacciari and G. P. Salam, Phys. Lett. B **641**, 57 (2006).
[45] M. Cacciari, G. P. Salam, and G. Soyez, Eur. Phys. J. C **72**, 1896 (2012).
[46] T. Gleisberg, S. Höche, F. Krauss, M. Schönherr, S. Schumann, F. Siegert, and J. Winter, J. High Energy Phys. 02 (2009) 007.
[47] P. Z. Skands, B. R. Webber, and J. Winter, J. High Energy Phys. 07 (2012) 151.
[48] S. Schumann and F. Krauss, J. High Energy Phys. 03 (2008) 038.
[49] S. Höche, S. Schumann, and F. Siegert, Phys. Rev. D **81**, 034026 (2010).
[50] J. Pumplin, D. R. Stump, J. Huston, H.-L. Lai, P. Nadolsky, and W.-K. Tung (CTEQ Collaboration), J. High Energy Phys. 07 (2002) 012.
[51] R. M. Godbole, K. Rao, S. D. Rindani, and R. K. Singh, J. High Energy Phys. 11 (2010) 144.
[52] V. Barger, W.-Y. Keung, and C.-T. Yu, Phys. Rev. D **85**, 056008 (2012).
[53] E. L. Berger, Q.-H. Cao, C.-R. Chen, and H. Zhang, Phys. Rev. D **83**, 114026 (2011).
[54] E. L. Berger, Q.-H. Cao, C.-R. Chen, J.-H. Yu, and H. Zhang, arXiv:1111.3641.
[55] G. Marques Tavares and M. Schmaltz, Phys. Rev. D **84**, 054008 (2011).
[56] P. H. Frampton and S. L. Glashow, Phys. Lett. B **190**, 157 (1987).
[57] A. Djouadi, G. Moreau, F. Richard, and R. K. Singh, Phys. Rev. D **82**, 071702 (2010).
[58] M. Bauer, F. Goertz, U. Haisch, T. Pfoh, and S. Westhoff, J. High Energy Phys. 11 (2010) 039.
[59] C. Delaunay, O. Gedalia, S. J. Lee, G. Perez, and E. Ponton, Phys. Rev. D **83**, 115003 (2011).
[60] J. Aguilar-Saavedra and M. Perez-Victoria, Phys. Lett. B **705**, 228 (2011).
[61] Y. Bai, J. L. Hewett, J. Kaplan, and T. G. Rizzo, J. High Energy Phys. 03 (2011) 003.
[62] R. Barcelo, A. Carmona, M. Masip, and J. Santiago, Phys. Rev. D **84**, 014024 (2011).
[63] R. Barcelo, A. Carmona, M. Masip, and J. Santiago, Phys. Lett. B **707**, 88 (2012).
[64] E. Alvarez, L. Da Rold, J. I. S. Vietto, and A. Szynkman, J. High Energy Phys. 09 (2011) 007.
[65] C. Delaunay, O. Gedalia, S. J. Lee, G. Perez, and E. Ponton, Phys. Lett. B **703**, 486 (2011).
[66] L. Da Rold, C. Delaunay, C. Grojean, and G. Perez, arXiv:1208.1499.
[67] J. Alwall, M. Herquet, F. Maltoni, O. Mattelaer, and T. Stelzer, J. High Energy Phys. 06 (2011) 128.
[68] J. D. Lykken, A. Martin, and J. Winter, J. High Energy Phys. 08 (2012) 062.